ASTRONOMY
AND
ASTROPHYSICS

A Representative Sample of Be Stars IV: Infrared Photometry and the Continuum Excess

Lee Howells, I.A. Steele, John M. Porter and J. Etherton

Astrophysics Research Institute, Liverpool John Moores University, Egerton Wharf, Birkenhead, CH41 1LD, United Kingdom

Abstract. We present infra-red (JHK) photometry of 52 isolated Be stars of spectral types O9–B9 and luminosity classes III–V. We describe a new method of reduction, enabling separation of interstellar reddening and circumstellar excess. Using this technique we find that the disc emission makes a maximum contribution to the optical $(B - V)$ colour of a few tenths of a magnitude. We find strong correlations between a range of emission lines (Hα, Brγ, Br11, and Br18) from the Be stars' discs, and the circumstellar continuum excesses. We also find that stellar rotation and disc excess are correlated.

Key words: Stars: emission-line, Be – circumstellar matter – Stars: rotation – Techniques: photometric – Methods: data analysis

1. Introduction

Classical Be stars are observed to be rotating close to their break up speeds (Slettebak 1982) with a modal value of $\sim 0.7v_{crit}$ (Porter 1996), where v_{crit} is the stars' critical break-up velocities. The distribution of circumstellar material giving rise to the emission features in their spectra (leading to their designation "e") is concentrated in the equatorial plane (Dougherty & Taylor 1992, Quirrenbach et al. 1994). Emission line profiles, *e.g.* see Dachs et al. (1986), Hummel & Vrancken (2000) are most easily explained if it is assumed that there are Keplerian motions within a disc. Observations of Be star discs have shown that some can vanish and re-appear in a apparently random fashion with time-scales of 100s of days (*e.g.* Hirata 1995, Hanuschik et al. 1993). The major problem in Be star research is to identify the physical processes which produce and disperse the discs.

Theoretical models which have been presented include wind bi-stability (Lamers & Pauldrach 1991), wind compressed discs (Bjorkman & Cassinelli 1993), and viscous outflowing discs (Lee et al. 1991, also see Porter 1999).

Each of these models has problems: the wind models (bi-stability and wind compression) cannot reproduce the Keplerian rotation in the disc as the wind conserves angular momentum leading to a rotation law similar to $v_\phi \propto 1/r$ (see Owocki et al. , 1994). Viscous outflowing discs successfully reproduce most of the attributes of the observed Be star discs (*e.g.* continuum excess Porter 1999, V/R variations in the emission lines Okazaki 1997), although the major problem is that the required source of angular momentum to sustain the disc remains obscure (a tentative suggestion has been made that the angular momentum source relates to non-radial pulsations, Osaki 1986).

Consequently our understanding of Be stars is still incomplete. Theoretical models can only be constrained, or indeed ruled out, if their predictions can be confronted with observations of well understood Be star samples. Hitherto, a homogeneous data set involving extensive wavelength coverage across all Be spectral types has been lacking.

In a series of papers we have been addressing that demand by defining and observing in a homogeneous fashion a representative sample of Be stars. The sample contains objects from O9 to B8.5 and of luminosity classes III (giants) to V (dwarfs), as well as three shell stars. It was selected in an attempt to contain several objects that were typical of each spectral and luminosity class in the above range; it therefore does *not* reflect the spectral and luminosity class space distribution of Be stars, but only the average properties of each subclass in temperature and luminosity. A spectral type and measure of $v \sin(i)$ were derived for each object in the sample and were presented in Steele et al. (1999, hereafter Paper I). In Clark & Steele (2000, hereafter Paper II) we presented K band spectroscopy of the sample, and in Steele & Clark (2000, hereafter Paper III) H band spectroscopy. In a forthcoming paper, Steele & Negueruela (2001, hereafter Paper V) will present spectra in the regions of the Hα and Paschen series lines.

This paper presents infrared JHK photometry of the sample and a new technique for separating out the interstellar reddening and circumstellar excess. We then go on to correlate the derived circumstellar excess of the ob-

jects in the sample their emission line strengths, spectral types and rotational velocities. Throughout this paper we shall be using non-parametric correlation analysis (using the Spearman rank correlation coefficient; *e.g.* Press et al. 1992) to study these relationships. In this way we impose no assumptions about the form of the dependence between parameters.

In section 2 we describe our observations and how we carried out the preliminary data reduction. Section 3 describes the process we have used to separate the circumstellar excess and interstellar reddening associated with observations of Be stars. In section 4 we present the correlations we have found between the separated excesses, reddenings and other observed quantities. Finally Section 5 presents our conclusions.

2. The Observations

Infrared photometry of the sample was obtained on the nights of 1999 September 28–30 the using 155cm Carlos Sanchez Telescope (TCS) equipped with the CVF photometer. The filters used were the JHK filters of the TCS system (see Alonso et al. 1998). Standard stars taken from the UKIRT bright standards list (the UKIRT system is that defined by the UKIRT standards list, observed by the UKT9 photometer) were observed at high and low air masses roughly once per 90 minutes. The standard methods of photometric data reduction were applied, with airmass corrections derived on a per filter, per night basis. Colour corrections from Alonso et al. (1998) and Leggett (1992) were used to convert the UKIRT standard magnitudes to the TCS system for reduction. After reduction in the TCS system, the final magnitudes were then converted to the standard CIT system (Elias et al. 1982), and it is these magnitudes that we present in Table 1. For those stars observed more than once we give a mean value, with the number of observations identified in brackets after each entry. The original sample contains 58 Be stars from O9→B8.5, however because of observational constraints the sample has been reduced, in this paper, to 52 objects.

3. Methodology - Separating the Interstellar Reddening and Circumstellar Excess

The flux from a star is reduced by interstellar extinction by a factor $(\exp[-\tau_{ext}(\lambda)])$, where $\tau_{ext}(\lambda)$ is the extinction optical depth. In general, if we have knowledge of the spectral type of the object (and hence its intrinsic colour) and the observed colours, then we can remove extinction effects from data using an interstellar extinction law (*e.g.* Rieke & Lebofsky 1985). However Be stars are well known to exhibit an infrared continuum excess, caused by free-free and free-bound emission within the disc, as well as the usual interstellar reddening (*e.g.* Gehrz et al. 1974). At first sight it appears not to be possible to separate the
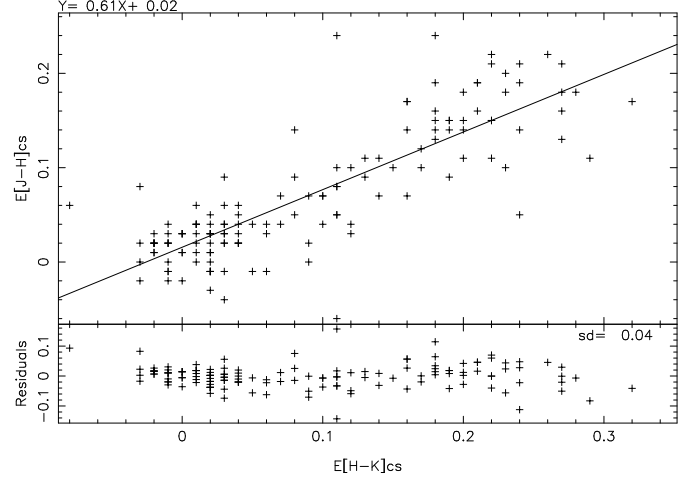
Fig. 1. Data extracted from Dougherty et al. (1994). The ratio β was calculated by means of a least squares fit, shown above as a solid line. Note that "sd" is the r.m.s. deviation of the residuals about the fitted line in the ordinate axis.

interstellar and circumstellar components using infrared photometry alone. However by using the fact that the spectral indices of the two components are different, we find that a deconvolution is possible as follows:

The observed colour, $(M_{\lambda_1} - M_{\lambda_2})_{obs}$, of a Be star consists of three components - the star's intrinsic colour, $(M_{\lambda_1} - M_{\lambda_2})_0$, the excess due to circumstellar material, $E(M_{\lambda_1} - M\lambda_2)_{cs}$ and the interstellar reddening, $E(M_{\lambda_1} - M_{\lambda_2})_{is}$. Using our JHK filters we can construct two observed colours:

$$(J - H)_{obs} = (J - H)_0 + E(J - H)_{cs} + E(J - H)_{is} \quad (1)$$

$$(H - K)_{obs} = (H - K)_0 + E(H - K)_{cs} + E(H - K)_{is} \quad (2)$$

A unique solution for these equations is possible by assuming a universal interstellar reddening law of the form:

$$E(J - H)_{is} = \alpha E(H - K)_{is}, \quad (3)$$

and also by assuming that the colours of the disc around the Be star can be related in a similar fashion (see, for example Figure 5 from Dougherty et al. 1994, re-plotted, with a least squares fit applied as our Figure 1):

$$E(J - H)_{cs} = \beta E(H - K)_{cs}. \quad (4)$$

The value of α may be simply derived from the interstellar extinction law of Rieke & Lebofsky (1985), giving $\alpha = 1.7 \pm 0.1$. To derive β, we use the circumstellar excesses of Be stars measured by Dougherty et al. (1994)

Star	Spec. type	EW Na(Å)	J	±Jerr	H	±Herr	K	±Kerr	(10)	(11)	(12)
BD+28 03598 (2)	O9II	−1.18	7.31	0.01	7.09	0.01	6.99	0.01	0.23	-0.08	1.18
BD+27 00797 (3)	B0.5V	-	9.74	0.03	9.44	0.01	9.38	0.01	0.31	-0.02	1.59
BD+57 00681	B0.5V	−0.00	7.63	0.01	7.43	0.01	7.39	0.01	0.23	-0.15	1.17
BD+37 03856	B0.5V	−0.48	9.47	0.02	9.34	0.01	9.39	0.01	0.21	-0.23	1.11
BD+56 00484 (2)	B1V	−1.15	8.55	0.02	8.34	0.01	8.11	0.01	0.12	0.14	0.64
BD+55 00605 (3)	B1V	−1.16	9.37	0.05	9.34	0.01	9.37	0.05	0.15	-0.09	0.78
BD+36 03946	B1V	−0.71	7.28	0.01	7.06	0.01	6.81	0.01	0.11	0.18	0.58
BD+56 00478 (2)	B1.5V	−1.15	7.86	0.01	7.66	0.01	7.46	0.01	0.12	0.13	0.60
BD+56 00573 (2)	B1.5V	−0.95	8.46	0.01	8.02	0.01	7.50	0.01	0.17	0.39	0.89
BD+29 04453	B1.5V	−0.40	7.79	0.01	7.68	0.01	7.42	0.01	0.02	0.27	0.11
BD+45 00933	B1.5V	−0.93	7.47	0.01	7.40	0.01	7.37	0.01	0.10	-0.04	0.51
BD+58 02320	B2V	−0.01	8.79	0.01	8.63	0.01	8.49	0.02	0.12	0.06	0.62
BD+42 01376 (2)	B2V	−0.39	6.99	0.01	6.88	0.01	6.74	0.01	0.06	0.12	0.31
BD+05 03704	B2.5V	−0.38	6.13	0.01	6.21	0.02	6.22	0.02	-0.03	0.05	-0.13
BD+47 00183	B2.5V	−0.19	4.43	0.03	4.37	0.02	4.22	0.02	0.04	0.14	0.19
BD+47 00939	B2.5V	−0.13	3.93	0.03	3.82	0.02	3.72	0.02	0.08	0.07	0.41
BD+42 04538 (2)	B2.5V	−0.89	7.78	0.02	7.67	0.01	7.49	0.01	0.05	0.16	0.27
BD+55 00552 (2)	B4V	−0.51	8.31	0.02	8.30	0.02	8.24	0.01	0.01	0.07	0.07
BD+30 03227 (3)	B4V	−0.36	6.82	0.03	6.88	0.02	6.94	0.02	0.02	-0.06	0.12
BD+50 00825 (2)	B7V	−0.23	6.02	0.01	5.92	0.01	5.91	0.01	0.09	-0.06	0.46
BD−02 05328	B7V	−0.14	6.32	0.03	6.34	0.02	6.33	0.02	-0.01	0.04	-0.06
BD+37 00675	B7V	−0.32	6.21	0.03	6.18	0.02	6.15	0.02	0.03	0.02	0.13
BD+58 00554 (2)	B7V	−0.74	8.53	0.01	8.43	0.01	8.33	0.01	0.05	0.06	0.27
CD−22 13183	B7V	−0.48	7.23	0.01	7.13	0.01	7.04	0.01	0.05	0.05	0.27
BD−00 03543 (2)	B7V	−0.42	6.80	0.01	6.79	0.01	6.77	0.01	0.01	0.02	0.06
BD+27 03411	B8V	−0.09	5.25	0.03	5.33	0.02	5.35	0.02	-0.04	0.02	-0.18
BD+50 03430	B8V	−0.21	7.09	0.01	7.08	0.01	7.06	0.01	0.01	0.17	0.07
BD+55 02411 (3)	B8.5V	−0.07	7.39	0.01	7.28	0.01	7.21	0.01	0.05	0.00	0.27
BD+20 04449 (2)	B0III	−0.48	8.52	0.01	8.61	0.02	8.69	0.01	0.03	-0.06	0.16
BD+56 00511 (2)	B1III	−1.29	8.31	0.01	8.17	0.01	8.09	0.01	0.14	-0.02	0.72
BD+46 00275	B5III	−0.89	4.29	0.03	4.29	0.02	4.29	0.02	0.04	-0.02	0.20
BD+49 00614 (2)	B5III	−0.56	7.68	0.01	7.67	0.01	7.67	0.01	0.04	-0.02	0.23
BD−19 05036 (2)	B4III	−0.58	7.10	0.06	6.94	0.01	6.90	0.01	0.14	-0.07	0.51
BD+51 03091	B7III	-	6.06	0.03	6.05	0.02	6.05	0.02	0.03	-0.01	0.13
BD+23 01148 (2)	B2III	−0.67	6.97	0.01	6.78	0.01	6.68	0.01	0.17	-0.03	0.89
CD−28 14778	B2III	−0.22	8.51	0.01	8.33	0.01	8.12	0.01	0.10	0.15	0.54
BD−12 05132 (2)	BN0.2III	−1.07	7.91	0.01	7.69	0.01	7.48	0.02	0.15	0.11	0.78
BD+47 03985	B1-2shell	−0.56	5.30	0.01	5.21	0.01	5.07	0.01	0.06	0.12	0.32
BD+43 01048 (3)	B6IIIshell	−1.29	8.90	0.02	8.80	0.01	8.71	0.02	0.08	0.03	0.39
BD+02 03815	B7-8shell	−0.72	6.58	0.03	6.57	0.02	6.53	0.02	-0.01	0.07	-0.03
CD−27 11872	B0.5V-III	-	6.89	0.01	6.59	0.01	6.28	0.01	0.17	0.19	0.86
BD+29 03842 (3)	B1II	−1.40	9.10	0.01	8.98	0.02	8.92	0.01	0.14	-0.07	0.73
BD+56 00493 (3)	B1V-IV	−0.74	9.35	0.02	9.27	0.02	9.24	0.02	0.11	-0.04	0.57
BD+27 00850	B1.5IV	−0.76	8.98	0.02	8.91	0.01	8.92	0.02	0.13	-0.10	0.65
BD+56 00473 (2)	B1V-III	−0.87	8.04	0.01	7.78	0.01	7.44	0.01	0.11	0.13	0.57
BD−01 03834	B2IV	−0.39	7.67	0.03	7.59	0.02	7.40	0.02	0.01	0.22	0.08
BD+40 01213 (2)	B2.5IV	−0.42	7.50	0.01	7.50	0.01	7.50	0.01	0.03	0.01	0.17
BD+47 00857	B4V-IV	-	4.17	0.03	4.04	0.02	3.88	0.02	0.07	0.12	0.37
BD+21 04695	B6III-V	−0.32	5.91	0.03	5.95	0.02	5.97	0.02	0.01	-0.01	0.03
BD+17 04087	B6III-V	−0.69	9.75	0.03	9.72	0.02	9.66	0.02	0.02	0.07	0.08
CD−27 16010	B8IV	-	4.24	0.03	4.25	0.02	4.24	0.02	0.03	-0.04	0.16
BD+31 04018	BB1.5V	−0.69	6.64	0.03	6.51	0.02	6.33	0.02	-0.07	0.39	-0.36

Table 1. Our full data sample showing respectively the object, with multiple observations in brackets and spectral type. The Na D_2 5890Å line EW, JHK photometry post reduction with their associated errors, the results of our separation procedure as $E(H − K)_{is}$ (column 10) & $E(H − K)_{cs}$ (column 11) and the IR colour $(H − K)$ converted to an equivalent optical $(B − V)$ colour as $E(B − V)_{(H−K)_{is}}$ (column 12)

who de-redden their photometry based on a combination of the reddening free Geneva system parameters X and Y, and the strength of the interstellar 2200 Å feature in IUE spectra. A least squares fit to the data, giving a $\chi^2_{reduced} = 1.02$, presented in their Figure 5 gives $\beta = 0.61 \pm 0.02$ (see Figure 1). We note that the r.m.s. deviation in the ordinate direction of the graph, $E[J-H]_{cs}$ vs $E[H-K]_{cs}$ is $sd = 0.04$, while that for the graph $E[H-K]_{cs}$ vs $E[J-H]_{cs}$ is $sd = 0.05$. we are therefore confident that a 1D minimisation is sufficient. We note also that a Spearman rank correlation test gives a Spearman rank coefficient, $r = 0.8$, when applied to this data, implying a high correlation between the circumstellar excess colours.

By combining equations 1 to 4 we are able to analytically solve to separate the interstellar and circumstellar components. We find:

$$E(H-K)_{is} = \frac{(H-K)_{obs} - \frac{1}{\beta}(J-H)_{obs} - (H-K)_0 + \frac{1}{\beta}(J-H)_0}{(1-\frac{\alpha}{\beta})} \quad (5)$$

$$E(H-K)_{cs} = \frac{(H-K)_{obs} - \frac{1}{\alpha}(J-H)_{obs} - (H-K)_0 + \frac{1}{\alpha}(J-H)_0}{(1-\frac{\beta}{\alpha})} \quad (6)$$

$$E(J-H)_{is} = \frac{(J-H)_{obs} - \frac{1}{\beta}(H-K)_{obs} - (J-H)_0 + \frac{1}{\beta}(H-K)_0}{(1-\frac{\beta}{\alpha})} \quad (7)$$

$$E(J-H)_{cs} = \frac{(J-H)_{obs} - \frac{1}{\alpha}(H-K)_{obs} - (J-H)_0 + \frac{1}{\alpha}(H-K)_0}{(1-\frac{\alpha}{\beta})} \quad (8)$$

The intrinsic colours $(H-K)_0$ and $(J-H)_0$ come from Koornneef (1983). The solutions of equations 5–6 are tabulated in Table 1. We present only the $(H-K)$ solutions because the $(J-H)$ results are not independent, the ratios α and β relating the two. Colour excesses for $(J-H)$ can be simply calculated using equations 7–8.

The errors generated from our calculations are twofold, (i) random errors from our observational data and the intrinsic colours, which enables us to construct errors and quantify the scatter and (ii) systematic errors from the ratios α and β, which shift the calculated best fit lines to their upper and lower extremities. We calculate a systematic error of $\sim 5\%$ in $E(H-K)_{cs}$ and $\sim 4\%$ in $E(H-K)_{is}$.

In order to test our de-reddening procedure, we compare the measured interstellar reddening to an independent measure of the same quantity. For this we use equivalent width[1] (EW) of the interstellar sodium D_2 5890Å line, listed in column 3 of Table 1. We note that there is an error of 10% on the Na EW. This was measured from the red optical spectra of the sample (see Paper V) using the FIGARO routine ABLINE. In Figure 2 we plot the EW of this line against our derived interstellar reddening and circumstellar excess. As expected there appears to be a correlation with $E(H-K)_{is}$ although not with $E(H-K)_{cs}$.

_____
[1] Note that in this paper we will employ the convention that *positive* equivalent widths indicate *emission* features.

To quantify this we performed non-parametric correlation tests (Spearman rank). The results for all such tests carried out in this paper are presented in Table 2. We note here that Spearman rank correlation confidences are normally compared with a critical correlation coefficient, r_s, which imply a significance level for the correlation. we list this significance level for each test in Table 2. However we have also chosen to express our results as a standard deviation (σ) measure (confidence level) to allow easy comparison with parametric tests. Implicit in this is the assumption that repeated tests of similar samples would find a normal distribution of the derived correlation coefficients. To derive this confidence level we used the one-tailed r_s lookup tables of Wall (1996) to find the significance level and then the one-tailed normal distribution lookup tables of Wall (1979) to find the confidence levels. Therefore we also list in Table 2 the confidence level of each test. The positive correlation between sodium EW and the interstellar extinction is confirmed at a $> 4.5\sigma$ confidence level while any correlation between sodium and $E(H-K)_{cs}$ is at a confidence level of less than 1σ. This result gives us confidence that our method does indeed separate the interstellar and circumstellar components of the infrared excess.

To quantify the strength of any optical circumstellar excess in our sample we convert our IR interstellar excesses to equivalent optical data using our adopted interstellar extinction law of Rieke & Lebosky (1985). The interstellar excess converted from an $(H-K)$ colour to a $(B-V)$ equivalent colour is denoted by $E(B-V)_{(H-K)_{is}}$. This is plotted against $E(B-V)_{cs+is}$, *i.e.* incorporating both interstellar reddening and circumstellar excess (see Figure 4), where $\Delta E(B-V)_{(H-K)_{is}} \gg \Delta E(B-V)_{is+cs}$ and so it is $E(B-V)_{(H-K)_{is}}$ that has been minimised. $E(B-V)_{cs+is}$ is derived from historical observational data (see Paper I) and the intrinsic $(B-V)$ colours of B stars (Cramer 1984). An independent test of our de-reddening procedure may now be carried out if we assume a negligible circumstellar excess for the optical $(B-V)$ colour: The colour-colour plot should produce a one-to-one correlation if the assumption of zero optical excess is true. A correlation is again obvious ($r = 0.74$), and we note that no significant offset between the two measures of reddening is apparent.

This implies that the assumption of negligible optical circumstellar excess appears to be reasonable at the level of <0.17 magnitudes, (the intercept of Figure 4). There is also a systematic error (as described above) of 0.2mags associated with the plot in the ordinate direction. This implies boundary conditions of $-0.03 < E(B-V)_{cs} < 0.37$ magnitudes. A similar result was found by Dachs, Kiehling & Engels (1988) who find that the maximum contribution of circumstellar envelopes to observed $(B-V)$ colours in Be stars amounts to $E(B-V)_{cs} \sim 0.1$ magnitudes.

In the light of this result (negligible optical circumstellar excess) it would be interesting to determine which
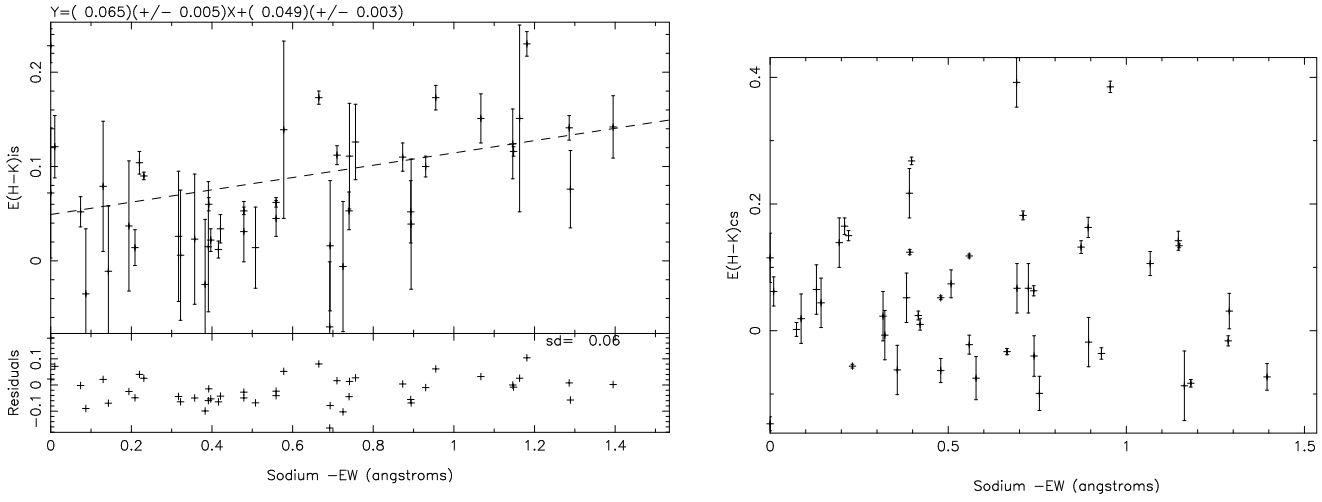
Fig. 2. Interstellar extinction versus Na D_2 5890Å line EW (left panel), where the fitted line is a least squares fit weighted to the ordinate axis errors, and versus circumstellar excess (right panel). Note that as expected no correlation between the *interstellar Na EW* and the *circumstellar* excess is present.
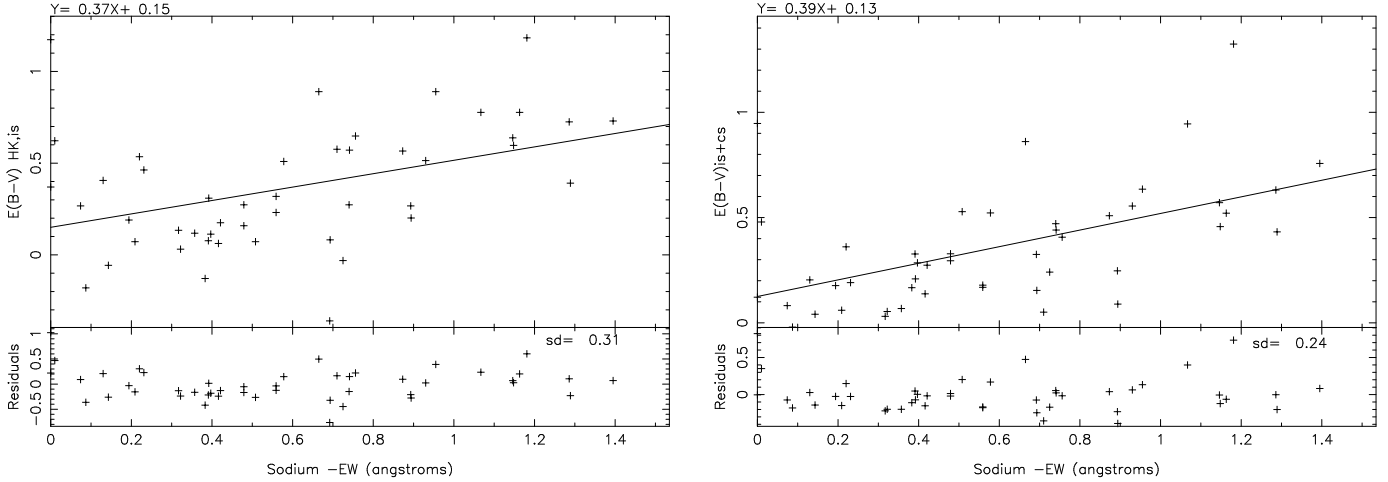
Fig. 3. (Left panel) a plot of $E(B-V)_{(H-K)_{is}}$, the IR $(H-K)$ interstellar reddening, converted to an optical $(B-V)$ colour versus sodium EW(Å). (Right Panel) a plot of $(B-V)_{is+cs}$ versus the Na D_2 5890Å line EW. The fitted lines are least squares fits minimised in the ordinate axis.

method (optical colours, infrared colours or sodium equivalent width) gives a better estimate of the interstellar reddening to Be stars. The Spearman rank correlation coefficient of $E(B-V)_{is+cs}$ versus the sodium EW (see Figure 3, right panel) is $r = 0.56$. For $E(B-V)_{(H-K)_{is}}$ versus sodium EW (Figure 3, left panel) the Spearman rank correlation coefficient is $r = 0.45$. However the greatest correlation is between $E(B-V)_{is+cs}$ and $E(B-V)_{(H-K)_{is}}$ (see Figure 4) with $r = 0.74$. In other words it appears that both the traditional optical and our new infrared method are more reliable than the sodium equivalent width for determining the interstellar reddening to Be stars. In the sections that follow we prefer to use our new method, as it is based on data taken closer in time (within a few years) to the spectroscopic data than the optical data (over 30 years in many cases).

4. Results

In this section we plot the separated $E(H-K)_{cs}$ against the equivalent widths of various emission features from the spectra presented in Papers II, III and IV and test to see if the quantities are related by using a Spearman rank test which is non-parametric. Where we believe a linear correlation exists we calculate best fit lines using a least squares fit weighted to errors in the ordinate axis. For each of these *linear* cases we display the calculated equations above each plot and the standard deviation, in the ordinate direction, about the fitted line in the residuals section of the plot. These values are also recorded in Table 2.

We removed the underlying photospheric absorption by combining our spectra with values of corresponding B star absorption lines tabulated in Hanson et al. (1996) and Hanson et al. (1998).

We note here two stars whose results do not conform with rest of the sample. When plotted in our *preliminary* results, specifically Figures 2(right panel), 5, 6, 8 & 9: BD+37 03856 has an anomalous spectral energy distribution (SED) for a Be star. Each of the other stars in our sample has a SED of the the form $J > H > K$ or $K > H > J$, where JHK are fluxes, however the SED of this star is such that $J > H < K$. This star also exhibited the most extreme point on our plots having the most negative $E(H-K)_{cs}$, we therefore remove the point from our plots but for completeness list the object in Table 1. A possible explanation for this SED is thermal emission from dust, although we note that the object is not in the IRAS point source catalogue.

BD+57 00681 also exhibits a large, negative $E(H-K)_{cs}$. The random error on this object is small at $< 1\%$ and it lies a long way from our calculated fit. We find no reason however to remove the point from the data set.

4.1. Brγ, Br11, Br18 and Hα

Our Brγ EW come from Paper II and have an error of $\sim 10\%$. Br18 EW and Br11 EW are extracted from Paper III and also have errors of $\sim 10\%$. Hα data come from Paper V and again have an error of $\sim 10\%$.

We plot the $E(H-K)_{cs}$ against Brγ, Br18, Br11 and Hα in Figures 5 and 6. There is an obvious correlation in each of the plots, re-enforced by the $> 4.5\sigma$ confidence levels produced by the Spearman tests. We fit lines of least squares, weighted to the ordinate axis errors, to the data in order to ascertain any linear correlation.

It is worthy of note that van Kerkwijk et al. (1995) present similar results to ours regarding the relationship between line equivalent width and continuum excess, although they present Hα versus J-L excess emission. In that study, as with our results there is a strong (apparently linear) correlation between the lines and continuum excess. This correlation is not surprising, as the hydrogen lines and the near-IR excess continuum are typically formed in the same regions of the disc. van Kerkwijk et al. (1995) also show the line-excess continuum correlations for two popular models of the disc – Waters' disc model (1986a), and the Poeckert & Marlborough model (PM) (1978) – and find that neither can replicate the results particularly well. The PM model produces too little line emission for a given continuum excess, and the disc model produces too much line emission, unless a large density gradient is used (a radial density power law with an index larger than 3.5 seems to be necessary which appears to be inconsistent with the results obtained from IRAS data). Whilst there is a large scatter in the data, we present the linear best-fit relationship from our results which any new model of Be star discs should attempt to reproduce.

4.2. Helium I 2.058μm

The HeI 2.058μm emission is confined to the early stars of the sample, being seen in 19 of the 34 stars with spectral types determined in Paper I to be earlier than B2.5. In Figure 7 we plot $E(J-H)_{cs}$ versus HeI 2.058μm. We note that data in Hanson et al. (1996) shows the absorption lines for the HeI 2.0581μm line to be negligible and so no correction has been made. Figure 7 has $r = 0.38$ and is therefore correlated at $> 4\sigma$ confidence level, although no linear correlation seems to exist. This is likely due to the fact that the HeI 2.058μm line is extremely sensitive to changes in the UV continuum and optical depth (Paper II).

4.3. Spectral Type

Figure 8 shows a plot of circumstellar excess against spectral type, we note that there appears to be no linear correlation and that $r = 4 \times 10^{-3}$ which gives a confidence level of $> 2\sigma$. However, the overall shape of the distri-
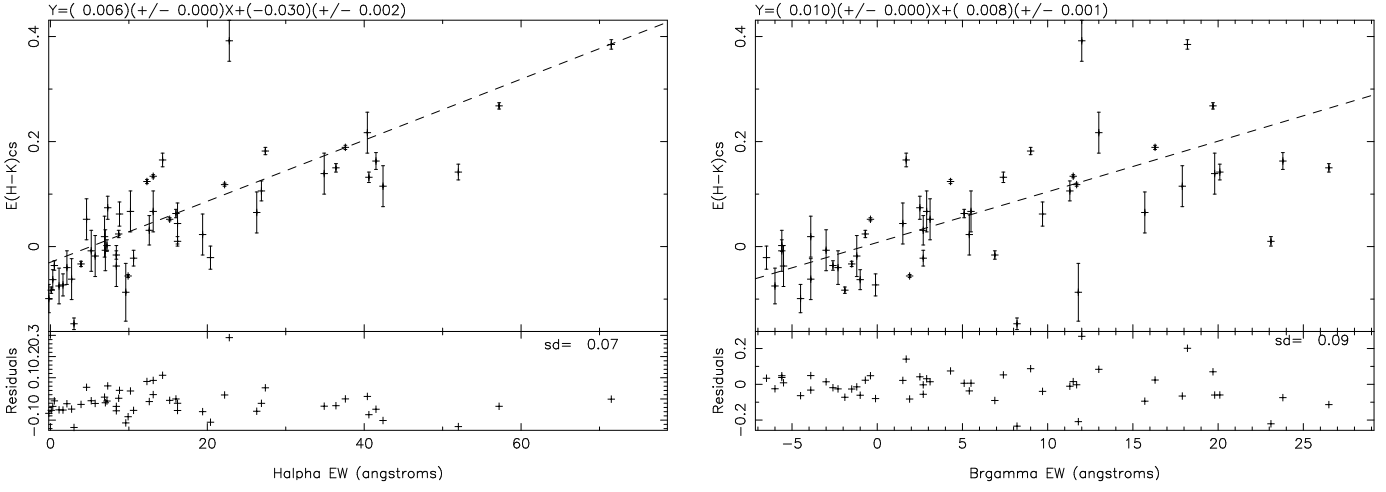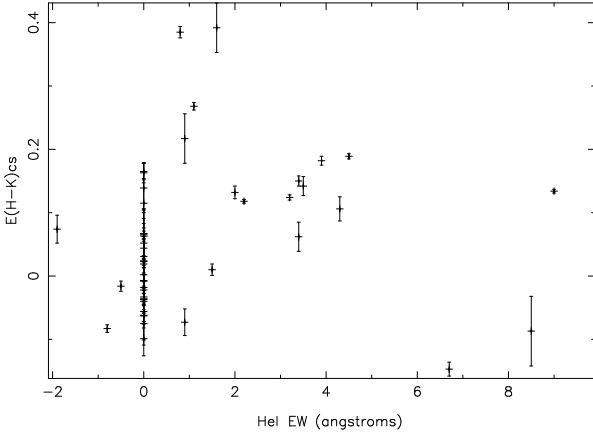
Fig. 5. Circumstellar excess versus $H\alpha$ EW/Å(left panel) and Brγ EW/Å(right panel). The fitted lines are least squares fits weighted to the ordinate axis errors
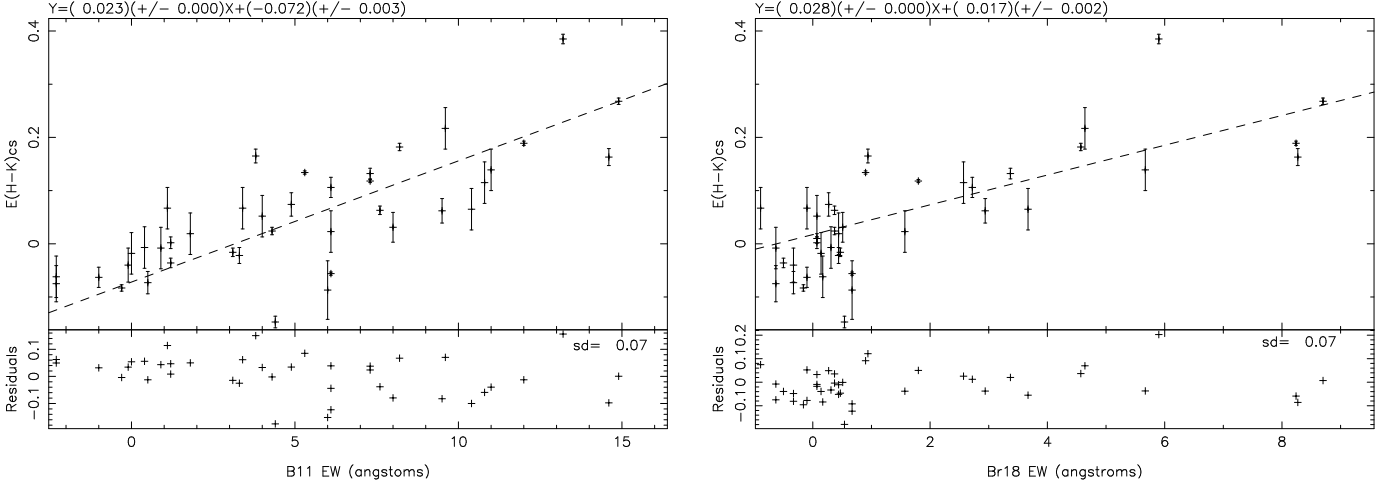
**Fig. 6.** Circumstellar excess versus Br11 EW/Å(left panel) and Br18 EW/Å(right panel). The fitted lines are least squares fits weighted to the ordinate axis errors
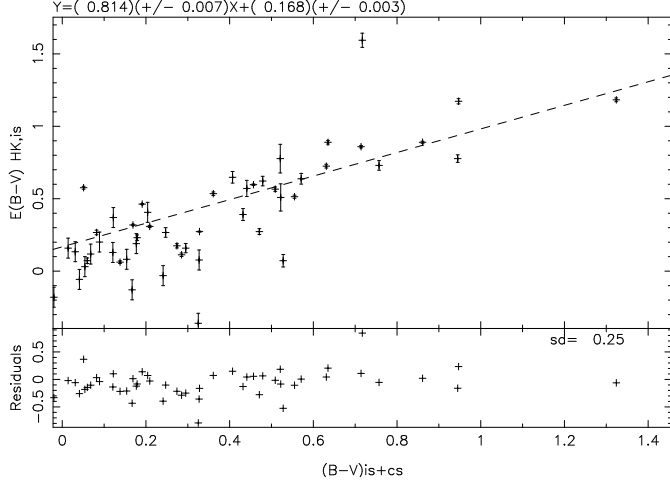
Fig. 4. A plot of $E(B-V)_{(H-K)_{is}}$ (the IR $(H-K)$ interstellar reddening converted to an optical $(B-V)$ colour) versus the optical $(B-V)_{is+cs}$ colour , which incorporates both interstellar reddening and circumstellar excess.

Fig. 7. Circumstellar excess versus HeI 2.058μm EW/Å
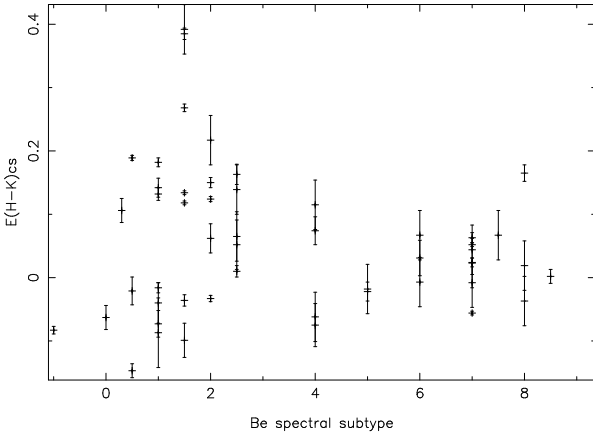
Fig. 8. Circumstellar excess versus spectral subtype

bution is similar to that seen in Paper II and Paper III for the strength of the Balmer series lines, with a broader range of excess around B1–B2. We note also that there is no correlation between luminosity class and circumstellar excess.

4.4. $v\sin(i)$ & $\omega\sin(i)$

Stellar rotation has been fundamentally linked with the generation of the Be phenomenon (*e.g.* Slettebak 1988, 1982). If rotation is the sole cause of the phenomenon then we would expect to see a strong correlation between rotational velocity and circumstellar excess. We therefore also plot $E(H-K)_{cs}$ versus $v\sin(i)$: see Figure 9, where velocity data are extracted from Paper I and Paper II. Dougherty et al. (1994), Waters (1986b) and Gehrz et al. (1974) all find a similar result, that there is no correlation between $v\sin(i)$ and colour excess. However from Spearman rank tests we are able say that $v\sin(i)$ and $E(H-K)_{cs}$ (see Figure 9, left panel) are related at a $> 4.5\sigma$ confidence level. In an attempt to remove spectral type dependence we also plot $\omega\sin(i)$ versus $E(H-K)_{cs}$, see Figure 9, right panel, where $\omega\sin(i) = v\sin(i)/v_{crit}$ with v_{crit} taken from Paper II, (see Porter 1996 for a discussion of the merits of using $\omega\sin(i)$ compared to $v\sin(i)$). While this plot exhibits a smaller scatter than our $v\sin(i)$ plot it is still correlated at confidence level of $> 4.5\sigma$.

5. Conclusions

We have presented IR (JHK) photometry of the "representative sample" of Be stars defined by Paper I. We have derived a new technique for separating the effects of (i) emission of the circumstellar material, and (ii) interstellar reddening. The technique involves combining photometry of 3 IR filters, a general interstellar extinction law and an assumption (that we verify) that the colours of the circumstellar disc of a Be star can be related in a similar fashion.

By correlating our results with an independent measure of interstellar reddening (the equivalent width of the Na I 5890Å line), we are confident that our method is valid. Using this technique we find that the disc emission makes a maximum contribution to the optical $(B - V)$ colour of a few tenths of a magnitude.

We find significant correlations between the infrared excess emission from the disc and emission from a range of lines (Hα, Brγ, Br11, and Br18). Linear fits to these correlations have been derived. There is also a significant correlation between the $v\sin(i)$ (and also $\omega\sin(i)$) of the Be star and the infrared disc emission. These data present strong constraints for models of the structure of Be stars. Any model that purports to explain their disc structure must be able to reproduce the correlations presented in
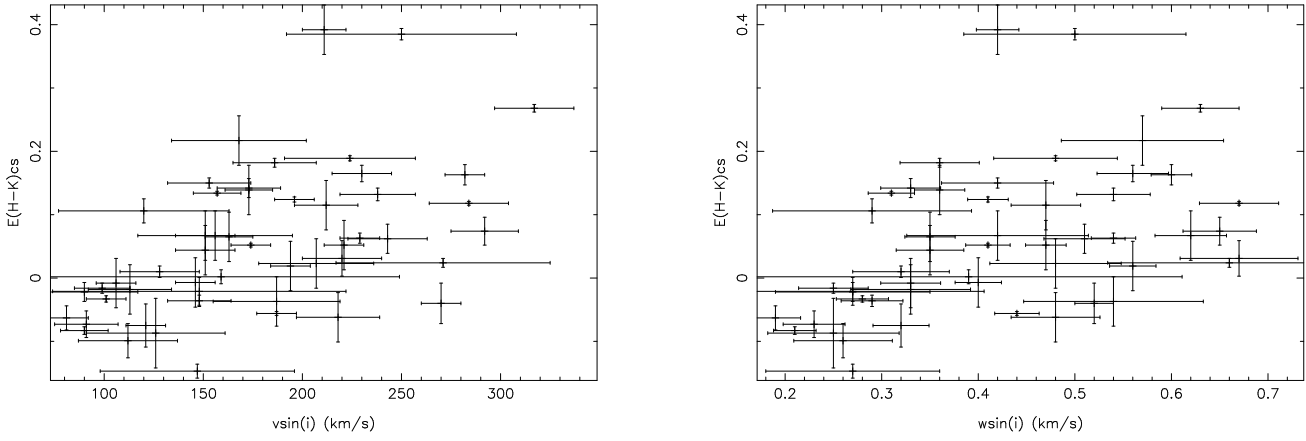
Fig. 9. Circumstellar excess versus $v\sin(i)$ (left panel) and $\omega\sin(i)$ (right panel).

Plot	r	Sig. level	Conf. level	Stan. dev.	Gradient	Intercept
$E(H-K)_{cs}$ vs $H\alpha$	0.83	0.005	$> 4.5\sigma$	±0.07	0.006 ± 0.000	-0.030 ± 0.002
$E(H-K)_{cs}$ vs Br11	0.75	0.005	$> 4.5\sigma$	±0.07	0.023 ± 0.000	-0.072 ± 0.003
$E(B-V)_{(H-K)_{is}}$ vs $E(B-V)_{is+cs}$	0.74	0.005	$> 4.5\sigma$	±0.25	0.814 ± 0.007	0.168 ± 0.003
$E(H-K)_{cs}$ vs Br18	0.70	0.005	$> 4.5\sigma$	±0.07	0.028 ± 0.000	0.017 ± 0.002
$E(H-K)_{cs}$ vs Brγ	0.69	0.005	$> 4.5\sigma$	±0.09	0.010 ± 0.000	0.008 ± 0.001
$E(H-K)_{cs}$ vs $v\sin(i)$	0.58	0.005	$> 4.5\sigma$	-	-	-
$E(H-K)_{cs}$ vs $\omega\sin(i)$	0.54	0.005	$> 4.5\sigma$	-	-	-
$E(B-V)_{is+cs}$ vs sodium EW	0.56	0.005	$> 4.5\sigma$	±0.24	0.39	0.13
$E(H-K)_{is}$ vs sodium EW	0.47	0.005	$> 4.5\sigma$	±0.06	0.065 ± 0.005	0.049 ± 0.003
$E(B-V)_{(H-K)_{is}}$ vs sodium EW	0.45	0.005	$> 4.5\sigma$	±0.31	0.37	0.15
$E(H-K)_{cs}$ vs HeI EW	0.38	0.37	$> 4\sigma$	-	-	-
$E(H-K)_{cs}$ vs spectral type	4×10^{-3}	$-$	$> 2\sigma$	-	-	-
$E(H-K)_{cs}$ vs sodium EW	-0.08	$-$	$< 1\sigma$	-	-	-

Table 2. We present our data table in order of descending Spearman rank coefficient, r (Col. 2), Col 3, sig. level, are the one-tailed significance levels of the Spearman rank Correlation and are extracted from Wall (1996). Col 4 are the one-tailed confidence levels of our correlations and are extracted from Wall (1979) and Col. 5 is the standard deviation about the fitted least squares fits line in the ordinate direction. In Col. 6 we present the gradient of those fits and Col. 7 is the intercept.

Figures 5–9. In a future study we will contrast these observations with predictions from current models.

References

Alonso A., Arribas S. Martinez-Roger, C. 1998, A&AS 131, 209

Bjorkman J. E. & Cassinelli J. P. 1993, ApJ 409, 429

Cramer N. 1984, A&A 132, 283

Clark J.S., Steele I.A., 2000, A&AS 141, 65 - Paper II

Dachs J., Kiehling R. Engels D. 1988, A&A 194, 167

Dachs J., Hanuschik R., Kaiser D. Rohe D. 1986, A&A 159, 276

Dougherty S.M., Waters L.B.F.M., Burki G., Cote J., Cramer N., van Kerkwijk M.H., Taylor A.R., 1994, A&A 290, 609

Dougherty S. M. Taylor A. R. 1992, Nature 359, 808

Elias J. H., Frogel J. A., Matthews K. Neugebauer G. 1982, AJ 87, 1029

Gehrz R.D., Hackwell J.A., Jones T.W., 1974, ApJ 191, 675

Hirata R. 1995, PASJ 47, 195

Hanson M.M., Conti P.S., Rieke, M.J., 1996, ApJs 107, 281

Hanson M.M., Rieke G.H., Luhman K.L., 1998, AJ 116, 1915

Hanuschik R. W., Dachs J., Baudzus M. Thimm G. 1993, A&A 274, 356

Hummel W. Vrancken M., 2000, A&A 359, 1075

van Kerkwijk M. H., Waters L.B.F.M., Marlborough J. M. 1995, A&A 300, 259

Kastner J.H. Mazzali, 1989, A&A 210, 295

Koornneef J., 1983, A&AS 128, 84

Lamers H.J.G., Pauldrach A.W.A., 1991, A&A 244, L5

Lee U., Osaki Y., Saio, H., 1991, MNRAS 250, 432

Leggett S. K. 1992, ApJ 82, 351

Okazaki A.T., 1997, A&A 318, 548

Osaki Y., 1986, PASP 98, 30

Owocki S.P., Cranmer S.R., Blondin J.M., 1994, APJ 424, 887

Poeckert R., Marlborough J.M., 1978 ApJ 220, 940

Porter J.M., 1996, MNRAS 280, L31

Porter J.M., 1999, A&A 348, 512

Press W.H., Teukolsky S.A., Vetterling W.T., Flannery B.P., 1992, Numerical Recipes in C, The Art of Scientific Computing, 2nd edn. Cambridge Univ. Press.

Quirrenbach A., Buscher D.F., Mozurkewich D., Hummel C.A., Armstrong J.T., 1994, A&A 283, L13

Rieke G.H., Lebofsky M.J., 1985, ApJ 288, 618

Slettebak A., 1982, ApJS 50, 55

Slettebak, A., 1988, PASP 100, 770

Steele I.A., Negueruela I., Clark J.S., 1999, A&AS 137, 147 - Paper I

Steele I.A., Clark J.S., 2000, A&AS in press - Paper III

Steele I.A., Negueruela I., A&AS in prep., - Paper V

Waters L.B.F.M., 1986b, A&A 159, L1

Waters L.B.F.M., 1986a, A&A 162, 121

Wall J.V., 1979, QJRAS 20, 138

Wall J.V., 1996, QJRAS 37, 519